

AUTOMATED QUANTITATIVE AND QUALITATIVE ANALYSIS OF WHOLE NEUROBLASTOMA TUMOUR IMAGES FOR PROGNOSIS

Siamak Tafavogh, Qinxue Meng*, Daniel R. Catchpole†, Paul J. Kennedy*

*Centre for Quantum Computation & Intelligent Systems,
Faculty of Engineering and Information Technology,

University of Technology, Sydney, PO Box 123, Broadway, NSW 2007 Australia

†Biospecimen Research and Tumour Bank, Children's Cancer Research Unit,
The Kids Research Institute, The Children's Hospital at Westmead
Siamak.tafavogh@uts.edu.au

ABSTRACT

Manual quantitative and qualitative microscopic analysis of cancerous tumours is subject to inter-intra observer variability in pathology. Neuroblastoma is an infant cancer with one of the lowest survival rates. Choosing a proper therapeutic regime for the tumour is highly dependent on determining the tumour aggressiveness level which requires an extensive microscopic analysis. There is an urgent demand from pathologists for reducing the role of microscopic analysis in the process of prognosis and using an automated system to determine the tumour aggressiveness. In this paper, we develop an automated system to address this demand. We propose a novel four-stage hybrid algorithm. First, we develop novel whole slide image partitioning and zooming techniques. Second, we introduce an image enhancement technique to reduce the intensity variation within the tissue images. Third, we deploy a thresholding technique for segmenting the regions of interest. Fourth, we develop a prognosis decision making engine based on a robust clinical prognosis scheme to classify the aggressiveness level using the segmented regions of interest. The performance of the system is evaluated by a pathologist. The system is compared against a state-of-the-art system, and the results indicate a superiority for our system in grading the tumour with average F-measure 86.77%.

KEY WORDS

Neuroblastoma Tumour, whole slide image analysis, image enhancement, automated prognosis decision making.

1. Introduction

Cancer is the common term for all malignant tumours and Neuroblastoma is an embryonal tumour of the sympathetic nervous system [1]. Neuroblastoma accounts for 15% of childhood cancer deaths and the incidence peak is between 0 to 4 years [2]. Early diagnosis of low and intermediate risk neuroblastoma increases the survival chance of patients. The prognosis of Neuroblastoma Tumour (NT) is associated to several factors, and

microscopic grading for determining the tumour aggressiveness level is one of the most important.

Microscopic grading is the study of quantity and quality of the different histological regions within the tissues. Level of aggressiveness depends on degree of tumour maturation and differentiation. Several grading systems have been proposed for identifying the neuroblastoma degree of differentiation over the years. The Shimada grading scheme [2] is an accurate and popular system among pathologists for classifying neuroblastoma. It groups NTs into six different categories which among those undifferentiated and poorly differentiated categories require intensive quantitative and qualitative analysis. Analyzing the whole slide under the microscope is a time-intensive and error-prone task. As a result there is a demand from pathologists for a consistent and automated system that performs quantitative and qualitative analysis on the whole tumour to enhance the accuracy of prognosis for tumours [3, 4]. Higher prognosis accuracy results in determining the most appropriate therapeutic regime.

The aim of this paper is to develop an automated and robust system to perform quantitative and qualitative analysis throughout whole tissue slide images of NT. The system assists pathologists by determining the degree of differentiation of NTs. This means that the system classifies NTs into undifferentiated, poorly differentiated or other types. However, there are three main issues with developing such a system: 1) analyzing the whole tumour tissue slide, 2) low image quality of the tissue tumours and 3) making an accurate prognosis decision.

The first issue derives from the fact that pathologists identify different types of histological region under the microscope based on their color. The images that are used in the experiments in this paper are derived from H&E stained tissue glass slides. Hematoxylin & Eosin is the most widely used method because of its diagnostic capability which is enhanced by the strong contrast between structures of different composition. However, the main drawback of H&E stained images for computerized analysis is inconsistency in staining the same type of histological regions with a unique color. For example, two separate cellular regions in different locations of a slide may be stained with different shades of blue. The colour

variation reduces the performance of the system in detecting different types of histological regions. The second issue is the enormous size of the whole digital slide images. For histological analysis of a tissue it is necessary to evaluate the image under higher magnification than the initial. The size of each histological image is 1.5GB on average which imposes a intensive computational load on the system. Moreover, to accurately analyze the different histological regions, pathologists usually evaluate the slides on 10X, 20X or 40X magnifications under the microscope [5]. Automatically zooming into the images is a challenging task which plays an important role in achieving higher performance by the system. The third issue is designing an accurate prognosis decision-making engine to grade the NTs. Many automated systems do not answer the real clinical needs of biologists, because they do not follow an appropriate clinical prognosis scheme.

Several automated systems have been proposed for different biological purposes. For example, [6] extracts the gland from prostate tissue images using texture features for the gland components such as stroma, lumen and nuclei. The system then exploits the K-means clustering technique to group the components into three clusters. Finally, it grades the gland according to the ratios of the components. [7] proposed a system for automated localization, segmentation and grading of breast cancer nuclei using a neural network. The proposed neural network learns from the cluster shapes and it grows by creating a new cluster based on the previously identified clusters. [8] developed a computer aided diagnosis system for assisting pathologists in the grading of Follicular Lymphoma. The system identifies basic histological structures in the image and models the connected components of such regions using ellipses. A set with a wide range of features is constructed from this intermediate representation to characterize the tissue. Using this representation, the relative amounts and spatial distributions of these histological components are measured to determine the grade of the follicular lymphoma tumour.

A common issue with many automated systems and the above-stated systems is their sensitivity to the low quality of images and intensity variation between the histological regions within the images. This sensitivity reduces the accuracy of the system in the segmentation process. Moreover, the systems are incapable of analyzing the whole slide images, and they do not analyze the tumour under different magnifications. This means that a user must provide the images with an appropriate magnification for a histological analysis. Finally, they do not follow a clinical prognosis scheme for grading the tumours.

This paper proposes three main contributions: In the first contribution, we propose a whole slide image analysis technique with a novel multi-scaling algorithm for analyzing the tumour tissues under different magnifications. The algorithm divides the images into a number of square partitions. It then expands the spatial

domain of each partition and interpolates new pixels to the expanded spatial domains. In the second contribution, to enhance the quality of the image, we develop an algorithm in two stages, namely global and local intensity variation reduction techniques. The global approach reduces the intensity variation throughout the images. The local approach mosaics the images by grouping the constituent pixels of the same type of histological regions and unifying their intensity values. In contribution 3, we develop a prognosis decision making engine to classify the NTs into three categories namely, undifferentiated, poorly differentiated and others. To this end, we develop a set of computerized rules based on the robust clinical diagnosis scheme proposed by Shimada et al. [2].

The rest of this paper is organized as following. Section 2 indicates the biological domain of the research. Section 3 describes image acquisition and the deployed software. Section 4 explains the methodology, our proposed whole slide analysis algorithm, the proposed rescaling approach, the introduced pre-segmentation and segmentation algorithms. Section 5 shows the system validation approach. Section 6 illustrates the results and finally the last section contains the conclusion.

2. Biological Domain

Neuroblastoma tumours are embryonal malignancies of the sympathetic nervous system which originate from the neural crest. The prognosis of NT is related to several factors: 1) age of the patient, 2) location of the tumour, 3) surgical staging, and 4) microscopic grading [5]. The first three factors can usually be determined accurately and easily by pathologists; however, determining microscopic grading requires extensive analysis of different histological regions and histological structures within the tumour tissue under the microscope. Microscopic grading of neuroblastoma indicates the degree of differentiation of the tumour, which can be used to determine the aggressiveness level of the tumour. According to Shimada et al [2] there are six different categories for NT of which undifferentiated and poorly differentiated are the most aggressive types. Determination requires extensive qualitative and quantitative microscopic analysis. The main morphological features of these two types of NT are high cellularity and neuropil regions. Cellular regions are stained blue by H&E and neuropil regions are pink in the histological slides. Neuropil is a region between neuronal cell bodies in the gray matter of the brain and spinal cord. Poorly differentiated NT is a highly cellular tumour of which more than 2% of the tumour contains neuropil regions [2]. Undifferentiated NT is a highly cellular tumour with indiscernible neuropil regions [2]. The other types of NT have normal cellularity status. High cellularity is a marker for undifferentiated and poorly differentiated types only. Figure 1 indicates different types of NT.

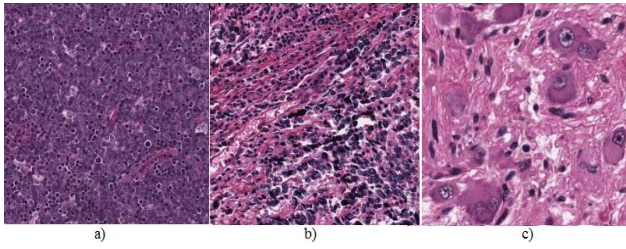


Figure 1 a) undifferentiated with high cellularity and indiscernible neuropil, b) poorly-differentiated with considerable neuropil, c) an example of one of the other types of NT with huge neuropil and normal cellularity.

3. Image Acquisition and Software

All of the images used in this research were provided by the Tumour Bank of The Kid's Research Institute at The Children Hospital at Westmead (CHW). All the images are derived from NTs. The Tumour Bank is compliant with national legislations and Declaration of Helsinki.

The dataset contains multiple tissue spots from multiple tissue arrays which are scanned by the Aperio ScanScope system. Figure 2 indicates a tissue array which contains 125 tissue spots. Different tissue spots contain different types of histological regions and histological structures and they are taken from different NTs. To construct the dataset, we crop 60 tissue spots in a way that the numbers of undifferentiated, poorly differentiated and other types are equal. Each of the test set and the training set contains 30 images of the tissue spots, and each of the sets contains 10 undifferentiated, 10 poorly-differentiated, and 10 other types of NTs. The format of the images is TIFF and their height and width are 5000X5000 pixels in average.

All the algorithms were developed using MATLAB (The MathWorks, Inc., Natic, MA) and experiments were run on a computer with 2X3.47 GHz processors and 12 GB RAM.

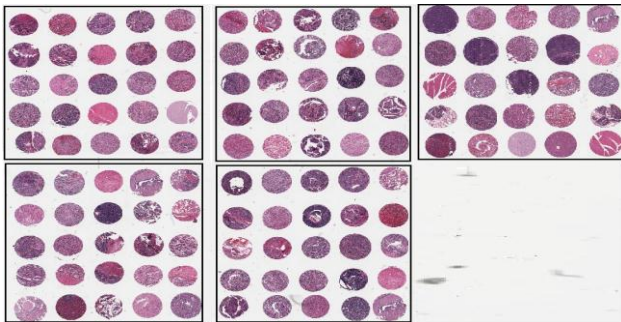


Figure 2 An example of a tissue array that is used in our experiments. (1X magnification).

4. Discussion

To classify the type of NT into undifferentiated, poorly-differentiated and others, the cellularity status of the tumour and the amount of neuropil regions must be determined. To this end, we propose a novel algorithm

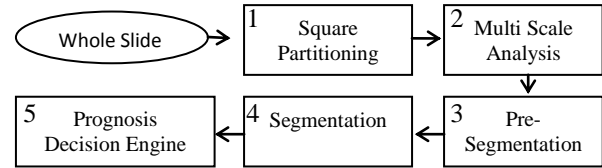


Figure 3 Overview of our system.

which contains five main sections as shown in Figure 3. The outcome of each of the sections is as following, 1) square partitioning: partitioning the whole slide images into several blocks of square shape to deal with the high computational load imposed by the huge size of images. 2) Multi-scale analysis: rescaling the images and analyzing them under different magnifications. 3) Pre-segmentation: enhancing the image quality by reducing the intensity variation. 4) Segmentation: locating and extracting the cellular regions and neuropil regions. 5) Prognosis decision engine: classifying NT into undifferentiated and poorly differentiated and other types based on the Shimada classification.

4.1 Whole Slide Analysis by Square Partitioning

To increase the accuracy of the prognosis it is necessary to analyze the whole tissue slide. We found that the size of each slide was 1.6GB on average, and an image with such an enormous size contains millions of pixels, which makes the image processing computationally expensive. To address this challenge we developed a square partitioning approach to divide the image into multiple sub-images, and we analyze them individually.

The size of original image is $n \times m$ where n is width and m is height of the image. Each image is partitioned into 25 square shaped blocks as shown in Figure 4. All the blocks are equal in size except the blocks at the last column and row which are indicated by blue solid line. To determine the size of blocks we calculate their width and height by $d = \lfloor \frac{n}{5} \rfloor$ and $k = \lfloor \frac{m}{5} \rfloor$ respectively. We consider the size of the first 16 blocks equal to $d \times k$. In Figure 4, the red dashed lines contains the first 16 blocks. We then compute the width and height of blocks at the last column and row by $i = n - 4d$ and $j = m - 4k$ respectively. Each of the constructed blocks is considered as an individual sub-image.

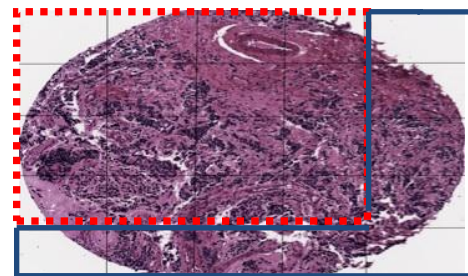


Figure 4 A partitioned image with 25 blocks. Squares within the red dashed line are all equal in size.

4.2 Multi Scale Analyses

The tumour tissues on the glass slides are fixed with their original size and this does not show their histological details. To analyze the histology of the tissues, pathologists must analyze them under higher magnification. Pathologists usually use 10X, 20X and 40X magnification for analyzing the tissue [5]. Thus, the system must zoom into the images for automatically analyzing the tissue histology. However, the main challenge is rescaling the image in such a way that it preserves the quality of the image and keeps the necessary details. As a result, we develop a two stage algorithm to rescale each of the sub-images obtained from our square partitioning as follows: 1) expanding spatial domain of the image, and 2) interpolating pixels to the empty spaces by assigning the associated intensity values to the new empty spaces.

4.2.1 Spatial Domain Expansion

We map the distribution of pixels in the original image to a matrix $O_{n \times m}$ where n and m are the total number of pixels in height and width of the image respectively. We then construct a new matrix $E_{x \times y}$ that contains the spatial coordinates of the pixels in the rescaled image, where $x = z * n$, $y = z * m$ and z is the magnification factor. All the pixels in O are transferred to their new spatial coordinates in E . For example, two neighbour pixels with coordinates $P_{(i,j)}$ and $P_{(i,j+1)}$ in matrix O are located at coordinates $P_{(z \times i, z \times j)}$ and $P_{(z \times i, z \times (j+1))}$ respectively. This means that between each two neighbour pixels in E there are $z-1$ empty slots.

4.2.2 Pixel Interpolation

To fill out the $z-1$ empty slots between the two neighbour pixels in E , we must determine their intensity values. To this end, we use the intensity values in O as following. Suppose $p_{(i,j)}$ and $p_{(i+1,j)}$ are two neighbour pixels in O . To calculate the intensity values for the $z-1$ empty slots between these two pixels in E , we use

$$v = \frac{|I(p_{(i,j+1)}) - I(p_{(i,j)})|}{z} \quad (1)$$

where $I(p)$ is the intensity value of the pixel p . We then fill the empty slot next to the pixel with the smaller intensity value by:

$$s_{x,y} = \min(I(p_{(i,j)}), I(p_{(i,j+1)})) + v \quad (2)$$

where x and y are the coordinates of the slot in E . Then the intensity values of the next empty slots are equal to the intensity values of the previous empty slots plus v . We repeat this until all slots between the two neighbour pixels receive their values. We apply the developed algorithm on each of the sub-images. The results of our experiments indicate that for 20X magnification ($z=20$), our system

achieves the highest accuracy in terms of making prognosis for NT with minimum mathematical expenses.

4.3 Pre-Segmentation

The low quality and the high intensity variation of the images significantly reduce the performance of locating and segmenting histological regions. Thus, before histological analysis the issues with the image quality must be addressed. To this end, we develop a novel algorithm that consists of two stages: global intensity variation reduction and local intensity variation reduction.

4.3.1 Global Intensity Variation Reduction

Using this technique we decrease the intensity variation throughout the entire image. To this end, the smallest RGB color cube which contains all the existing colors of the original image is found. Then the colors along the longest axis of the color cube are sorted using a median cut algorithm [9], which divides the longest axis of the color cube into two boxes at the median point. This process is repeated until the color cube has been divided into β boxes. Each of the boxes contains an approximately similar range of colors. All the colors falling into each box are mapped to the color value at the center of the box. The empirical results show that $\beta = 16$ provides the best performance. Figure 5 shows the outcome of our global intensity variation reduction technique.

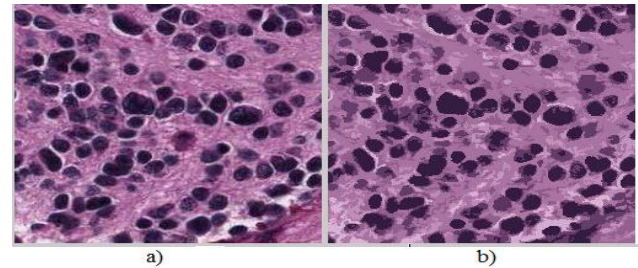


Figure 5 a) original image, b) global intensity variation reduction.

4.3.2 Local Intensity Variation Reduction

To reduce the intensity variations between the constituent pixels of the same histological regions, pixels with similar intensity and spatial domain are assigned to the same groups and we unify their intensity. To this end we propose a two stage algorithm partitioning the images into several mosaics and unifying the intensity variations within each of the mosaics.

Mosaicking the Image: The mosaicking technique divides the images into several areas. Each of the areas is constructed by homogeneous pixels in terms of the joint spatial-intensity domain. The spatial domain indicates the location of the pixel within the image and the intensity value indicates the color of the pixel. Intensity of the pixels is one of the major criteria for grouping them. Thus, the pixels must be analyzed in a color-space that represents the intensity differences between the pixels in a

uniform way. As a result, we transform the initial color-space of the images, RGB, to $L^*u^*v^*$. In contrast to $L^*u^*v^*$, the RGB color-space is not perceptually uniform because differences between colors cannot be determined by mathematical relations.

We consider a feature-space for each pixel with 5 features, namely its x and y coordinates, and its L^* , u^* and v^* channels. To group the homogenous color pixels we deployed our modified mean-shift algorithm [10, 11]. We define the kernel $K(X)$ for the pixel in $L^*u^*v^*$ color-space as following:

$$K_{h_S, h_I}(X) = \frac{C}{h_S^2 h_I^3} k\left(\left\|\frac{X^S}{h_S}\right\|\right)^2 k\left(\left\|\frac{X^I}{h_I}\right\|\right)^2 \quad (3)$$

where C is the normalization constant, h_S is spatial bandwidth, h_I is intensity bandwidth, X^S is spatial domain of pixel X , X^I is the intensity value of a pixel in 3-d vector, and k is the profile of the kernel. We then

$$\hat{f}_{h_S, h_I}(X) = \frac{1}{n h_S^2 h_I^3} \sum_{i=1}^n k\left(\frac{X - X_i}{h}\right) \quad (4)$$

deploy a density estimator using the kernel $K(X)$ in (3) by: where X_i is the pixel i , in the image, and n is the total number of pixels. By employing the profile function k of the kernel, the density estimator in (4) becomes,

$$\hat{f}_{h_S, h_I, K}(X) = \frac{C_{k,2,3}}{n h_S^2 h_I^3} \sum_{i=1}^n k\left(\left\|\frac{X^S - X_i^S}{h_S}\right\|\right)^2 k\left(\left\|\frac{X^I - X_i^I}{h_I}\right\|\right)^2 \quad (5)$$

In mean shift, the modes of density lie where the gradient is zero [12], thus the gradient of density estimator in (5) becomes,

$$\frac{\hat{f}_{h_S, h_I, K}(X)}{\sigma^{X^S X^I}} = \frac{4C_{k,2,3}}{n h_S^2 h_I^3} \sum_{i=1}^n (X^S - X_i^S)(X^I - X_i^I) k'\left(\left\|\frac{X^S - X_i^S}{h_S}\right\|\right) k'\left(\left\|\frac{X^I - X_i^I}{h_I}\right\|\right) \quad (6)$$

then by defining,

$$g(X) = -k'(X) \quad (7)$$

the new kernel $G(X)$ is derived as

$$G(X) = C_{g,2,3} g\left(\left\|\frac{X^S}{h_S}\right\|\right) g\left(\left\|\frac{X^I}{h_I}\right\|\right) \quad (8)$$

where $c_{g,2,3}$ is the normalization constant. Then substituting $g(X)$ into (8) yields,

$$\frac{\hat{f}_{h_S, h_I, K}(X)}{\sigma^{X^S X^I}} = \frac{4C_{k,2,3}}{n h_S^2 h_I^3} \sum_{i=1}^n (X^S - X_i^S)(X^I - X_i^I) g\left(\left\|\frac{X^S - X_i^S}{h_S}\right\|\right) g\left(\left\|\frac{X^I - X_i^I}{h_I}\right\|\right) = \frac{4C_{k,2,3}}{n h_S^2 h_I^3} \left[g\left(\left\|\frac{X^S - X_i^S}{h_S}\right\|\right)^2 g\left(\left\|\frac{X^I - X_i^I}{h_I}\right\|\right)^2 \right] \times \quad (9)$$

$$\left[\frac{\sum_{i=1}^n (X^S X_i^I - X^I X_i^S - X_i^S X_i^I) g\left(\left\|\frac{X^S - X_i^S}{h_S}\right\|\right)^2 g\left(\left\|\frac{X^I - X_i^I}{h_I}\right\|\right)^2}{\sum_{i=1}^n g\left(\left\|\frac{X^S - X_i^S}{h_S}\right\|\right)^2 g\left(\left\|\frac{X^I - X_i^I}{h_I}\right\|\right)^2} \right] - X^S X^I$$

Using the expression in (9) the homogenous pixels in terms of joint intensity-spatial domains form a mosaic. This means each mosaic represents a specific histological region as shown in Figure 6.

Intensity Unification for Each Mosaics: The last step in pre-segmentation is to unify the different intensity values between the pixels of the same mosaic. To this end the mean intensity value of the constituent pixels of each mosaic is computed. Then the color of pixels in each mosaic is unified to the associated mean value. Figure 7 shows an image after applying pre-segmentation.

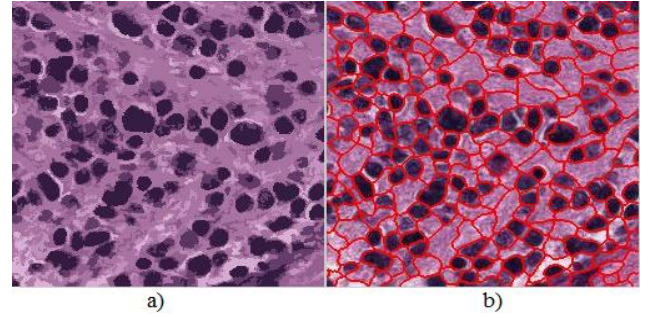


Figure 6 a) The image after global intensity unification, b) the constructed mosaics on the image.

4.4 Segmentation

Each histological region has a specific morphology in the tissue slide, and each has a correspondingly specific numerical pattern in the image. Segmentation techniques are used to locate and extract these numerical patterns. Because the main focus of this paper is not segmentation, we use the segmentation approach in [13] which deploys the well known, simple, yet efficient adaptive thresholding approach based on the Otsu method [14] for segmenting the cellular and neuropil regions. The Otsu method efficiently and accurately determines a different range of intensity values using the grey-level histogram of the pixels in the images with low range of intensity variation. Our proposed pre-segmentation technique reduces the intensity variations between the pixels in the images. Therefore, the Otsu method provides high performance in terms of segmenting the regions of interest. We apply the Otsu method to the Luminance channel (L^*) of the pixels only to find the optimum thresholding. The reason for this is that the Otsu method only analyzes the gray-level histogram of the pixels, and the two other channels provide chrominance information. The output of the segmentation is a binary foreground/background image where the foreground consists of constituent pixels of regions of interest such as cellular regions and neuropil regions and the background is 0. Figure 8 illustrates the results of segmenting cellular and neuropil regions.

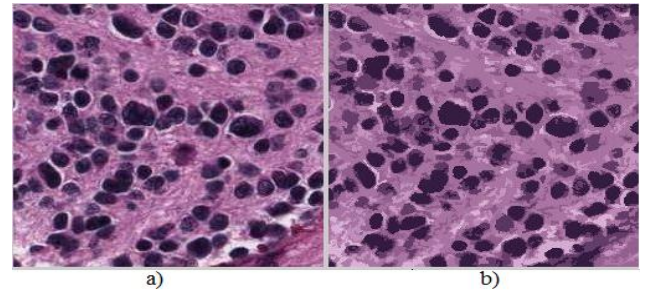


Figure 7 a) is the original image, and b) is the image after applying pre-segmentation.

4.5 Prognosis Decision Engine

We develop a prognosis decision making engine to analyze the information obtained from the segmented histological regions. To this end, we propose a set of

computerized rules based on Shimada scheme to classify the differentiation degree of NTs using the neuropil regions and cellular regions obtained by the segmentation. Figure 9 illustrates an overview of our prognosis engine.

To determine the amount of neuropil regions within the image, the prognosis engine calculates the ratio of neuropil regions to the summation of cellular regions and neuropil regions using the following expression:

$$NR = \frac{np}{cp + np} \quad (10)$$

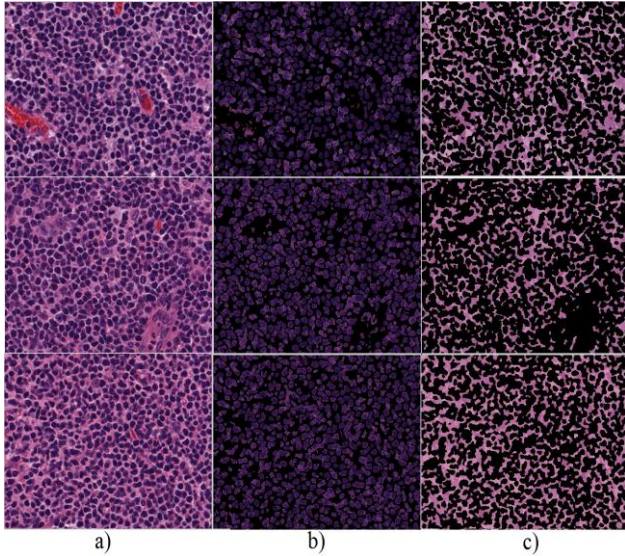


Figure 8 a) the input images, b) the segmented cellular regions, and c) the segmented neuropil regions.

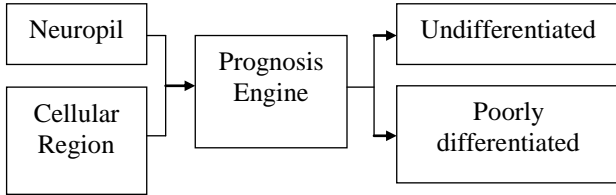


Figure 9 An overview of our prognosis decision engine.

where np is the total number of constituent pixels within the neuropil regions and cp is the total number of constituent pixels within the cellular regions.

To determine the cellularity status of the tumour, we first compute the ratio of the cellular regions in the tissue

$$CR = \frac{cp}{cp + np} \quad (11)$$

The cellularity status of the tumour is measured using

$$CS = \begin{cases} CR > T, & HC \\ otherwise, & Normal \end{cases} \quad (12)$$

where T is a threshold that discriminates the high cellular tumours from normal tumours. Pathologists estimate cellularity status of the tumours by eye and there is no predefined threshold value to discriminate high cellular tumours from normal tumours. As a result, we train our system based on decisions of two pathologists, one from

CHW and the other one an independent pathologist to tune $T=43.5$ empirically on the 30 training images. We used the training set of images for this purpose. We then developed Algorithm 1 to determine the type of NTs.

Algorithm 1 Classifying NT

Step 1:

Apply expression in (11) and (12) to determine the cellularity status of the tumour.

if Normal then NT ← Others.

otherwise, Step 2.

Step 2:

Apply expression (10) to determine the ratio of Neuropil regions.

if $NR > 0.02$ **then** NT ← Poorly-differentiated.

otherwise, NT ← Undifferentiated.

5. System Validation

All the results obtained by the system in this paper were validated by a pathologist from the Department of Histopathology in CHW, Sydney. The pathologist is considered as the ground truth and this is the baseline for all of the validations in this paper. To measure the performance of the proposed algorithm precision, recall and F-measure [15] of the obtained results are computed by comparing them with those of the pathologist. This means that the results of manual quantitative and qualitative analysis obtained by the pathologist are used as the ground truth for measuring the performance of the develop algorithm. A recent audit of the department of

Table 1

Confusion matrix for performance of our system in classifying NTs into undifferentiated (UD), poorly-differentiated (PD) and others.

Actual	Our Classification		
	UD	PD	Others
UD	8	1	1
PD	0	9	1
Others	1	0	9
Actual	Kong et al. Classification		
	UD	PD	Others
UD	7	2	1
PD	0	9	1
Others	2	0	8

histopathology at CHW shows 0% historical discordance in classifying NTs which indicates the quality of our ground truth. We also compare the performance of our system with the state-of-the-art system proposed by Kong et al. [16] in making prognosis for NTs. Lastly, to validate the performance of our zooming algorithm and image enhancement algorithms, we run several experiments by excluding our zooming technique, image enhancement

technique and combination of zooming and image enhancement techniques from our system in the process of NTs classification.

Kong et al. [16] proposed a similar system for classifying NTs by analyzing the whole slide. We also compare the results of our system with those of the Kong et al. to evaluate the performance of our system against the state-of-the-art systems. The system proposed by Kong et al. has been designed for analyzing H&E stained histological images, and it analyzes the whole slide tissue using a multi-resolution approach. The image at each resolution level is segmented into cellular, neuropil and background. To segment the histological structures, the system uses Expectation Maximization Linear Discriminant Analysis (EMLDA), that uses the joint intensity-entropy domain of pixels in the $L^*a^*b^*$ color-space images. Using this technique the constituent pixels of each of the histological regions are grouped into their associated cluster. Finally, the system grades NTs by combining a family of classifiers such as K-nearest neighbour, linear discriminate analysis, nearest mean, and support vector machine.

6. Results

To measure the performance of our proposed system in classifying NTs, we compare the results of our system with the ground truth. We also deploy the proposed system by Kong et al. on the test images. Table 1 reports the performance obtained by our system and the system proposed by Kong et al. in making a prognosis for NT in the form of confusion matrices. Table 2 indicates the

Table 2

Average precision, recall and F-measure obtained by our system and Kong et al. based on Table 2

	Our	Kong et al.
Precision	86.66%	80.00%
Recall	86.89%	79.86%
F-measure	86.77%	79.92%

average precision, recall and F-measure of both systems based on the confusion matrices in Table 1. The table shows that the average precision, recall and F-measure obtained by our system are higher than those of the Kong et al. system. This means that the system provides higher accuracy in classifying NTs into the undifferentiated, poorly-differentiated and others types. The inter-intra observer variability in pathology labs is approximately 20% [17] for the case of NT, while the table indicates that the error rate of our system is approximately 13%. This means that our system provides reliable results for pathology labs.

Also, to indicate the effects of our proposed zooming and image enhancement technique in the accuracy of NT classification, in Figure 10 we report the performance of our system when the zooming and the image enhancement algorithms are excluded. We run three experiments to

evaluate the performance of each of our developed algorithms.

In the first experiment, we apply our system to the test images without using the image enhancement algorithm. The figure indicates the decline in the performance of our system by excluding this algorithm. The main reason for this is that excluding our image enhancement algorithm increases the sensitivity of the system to low quality images and intensity variations. In the second experiment, we include image enhancement but exclude zooming algorithm. The figure indicates a significant decrease in precision, recall and F-measure of the system. This derives from the fact that to analyze the histology of the tissues, the original magnification does not provide enough details, and it must be analyzed under higher magnification. Lastly, we exclude both image enhancement and zooming algorithms from the system which provides the worse performance. The obtained results are lower than the results obtained by Kong et al. in this case.

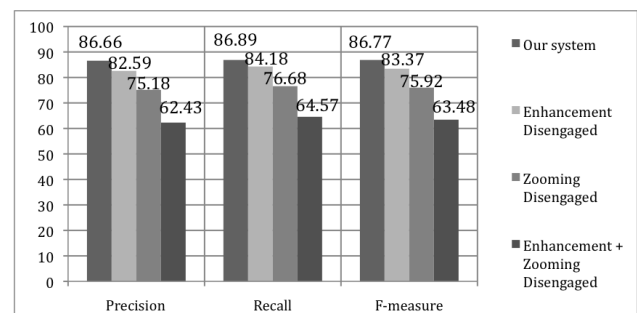


Figure 10 Effects of our developed zooming and image enhancement algorithms on the precision, recall and F-measure of our system in classifying NTs.

7. Conclusion

Prognosis of Neuroblastoma tumour is highly dependent on the microscopic analysis by pathologists. Two most aggressive types of NT namely undifferentiated and poorly-differentiated require extensive quantitative and qualitative microscopic analysis. The accuracy of NT classification has a significant effect on determining an appropriate therapeutic regime, and consequently, the survival chance of patients. This paper proposes a novel hybrid algorithm to analyze the whole slide NTs under different magnifications and to make a prognosis decision. The system classifies the NTs into Undifferentiated, Poorly-differentiated and Others types. To analyze the whole slide tumour, we introduce a square partitioning technique which divides the images into several blocks for reducing the computational load. To analyze in the scale of tissue histology, we develop a multi-scale analysis technique. This technique expands the size of images and enables the system to automatically zoom into the images for investigating details of histological regions. We also develop a novel image enhancement algorithm to reduce the intensity variations within the histological images. The algorithm consists of two stages: global and local intensity variation reduction techniques. The global technique

reduces the intensity level of the entire image in a way that it does not damage the significant data. The local technique reduces the intensity variations between the constituent pixels of the same histological regions. The results indicate that the proposed image enhancement technique reduces the sensitivity of our system to noisy and low quality images. For extracting the histological regions, namely cellular regions and neuropil regions, we deploy a simple but yet efficient adaptive thresholding technique based on the Otsu method. Lastly, we propose a prognosis decision making engine to make a prognosis and to classify the NTs into undifferentiated, poorly-differentiated and others types. The computerized rules for the prognosis engine are developed based on a well-known clinical classification scheme proposed by Shimada et al.

To validate the system, we compare the results obtained by our system in classifying NTs with those of a pathologist from CHW. Moreover, we compare the performance obtained by our system with that of the state-of-the-art system proposed by Kong et al. The precision, recall and F-measures obtained by our system exceed those of the state-of-the-art system. The obtained performance promises a reliable system which increases the accuracy of quantitative and qualitative analysis of NTs and reduces the inter-intra observer variability in pathology labs. Moreover, the system reduces work loads of pathologists by assisting them with performing a time taken task of tumour classification.

In future, we will extend our proposed algorithm in this paper to determine the specific morphological features which are related with diagnosis of NTs such as Mitosis and karyorrexhis rates.

References

- 1 Park, J.R., Eggert, A., and Caron, H.: 'Neuroblastoma: biology, prognosis, and treatment', *Pediatric clinics of North America*, 2008, 55, (1), pp. 97-120
- 2 Shimada, H., Ambros, I.M., Dehner, L.P., Hata, J.i., Joshi, V.V., and Roald, B.: 'Terminology and morphologic criteria of neuroblastic tumors', *Cancer*, 1999, 86, (2), pp. 349-363
- 3 Gurcan, M.N., Boucheron, L.E., Can, A., Madabhushi, A., Rajpoot, N.M., and Yener, B.: 'Histopathological image analysis: A review', *IEEE Reviews in Biomedical Engineering*, 2009, 2, pp. 147-171
- 4 Chetcuti, A., Mackie, N., Tafavogh, S., Graf, N., Henwood, T., Charlton, A., and Catchpoole, D.: 'Can Archival Tissue Reveal Answers to Modern Research Questions?: Computer-Aided Histological Assessment of Neuroblastoma Tumours Collected over 60 Years', *Microarrays*, 2014, 3, (1), pp. 72-88
- 5 Rosai, J.a.A., L. V.: 'Rosai and Ackerman's surgical pathology', *Ackerman's surgical pathology*, 2004
- 6 Farjam, R., Soltanian Zadeh, H., Jafari Khouzani, K., and Zoroofi, R.A.: 'An image analysis approach for automatic malignancy determination of prostate

- pathological images', *Cytometry Part B: Clinical Cytometry*, 2007, 72, (4), pp. 227-240
- 7 Lee, K.-M., and Street, W.N.: 'An adaptive resource-allocating network for automated detection, segmentation, and classification of breast cancer nuclei topic area: image processing and recognition', *IEEE Transactions on Neural Networks*, 2003, 14, (3), pp. 680-687
- 8 Sertel, O., Kong, J., Catalyurek, U.V., Lozanski, G., Saltz, J.H., and Gurcan, M.N.: 'Histopathological image analysis using model-based intermediate representations and color texture: Follicular lymphoma grading', *Journal of Signal Processing Systems*, 2009, 55, (1-3), pp. 169-183
- 9 Heckbert, P.: 'Color image quantization for frame buffer display' (*ASIGGRAPH Comput, Graph*, 1982. 1982)
- 10 Tafavogh, S., Kennedy, P.J., and Catchpoole, D.R.: 'Determining cellularity status of tumors based on histopathology using hybrid image segmentation', *The international joint conference on neural networks, IEEE*, 2012, pp. 1-8
- 11 Tafavogh, S., Navarro, K.F., Catchpoole, D.R., and Kennedy, P.J.: 'Non-parametric and integrated framework for segmenting and counting neuroblastic cells within neuroblastoma tumor images', *Medical & biological engineering & computing*, 2013, pp. 1-11
- 12 Comaniciu, D., and Meer, P.: 'Mean shift: A robust approach toward feature space analysis', *IEEE Transactions on Pattern Analysis and Machine Intelligence*, 2002, 24, (5), pp. 603-619
- 13 Tafavogh, S., Navarro, K.F., Catchpoole, D.R., and Kennedy, P.J.: 'Segmenting Neuroblastoma Tumor Images and Splitting Overlapping Cells Using Shortest Paths between Cell Contour Convex Regions': 'Artificial Intelligence in Medicine' (Springer, 2013), pp. 171-175
- 14 Otsu, N.: 'A threshold selection method from gray-level histograms', *Automatica*, 1975, 11, (285-296), pp. 23-27
- 15 Powers, D.M.: 'Evaluation: from precision, recall and F-measure to ROC, informedness, markedness & correlation', *Journal of Machine Learning Technologies*, 2011, 2, (1), pp. 37-63
- 16 Kong, J., Sertel, O., Shimada, H., Boyer, K.L., Saltz, J.H., and Gurcan, M.N.: 'Computer-aided evaluation of neuroblastoma on whole-slide histology images: Classifying grade of neuroblastic differentiation', *Pattern Recognition*, 2009, 42, (6), pp. 1080-1092
- 17 Teot, L.A., Sposto, R., Khayat, A., Qualman, S., Reaman, G., and Parham, D.: 'The problems and promise of central pathology review: development of a standardized procedure for the children's oncology group', *Pediatric and Developmental Pathology*, 2007, 10, (3), pp. 199-207